
Antarctic icebergs melt over the Southern Ocean : climatology and impact on sea ice

Merino Nacho ^{1,2,*}, Le Sommer Julien ^{1,2}, Durand Gael ^{1,2}, Jourdain Nicolas C. ^{1,2}, Madec Gurvan ^{3,4},
Mathiot Pierre ⁵, Tournadre Jean ⁶

¹ CNRS, LGGE, F-38041 Grenoble, France

² Univ. Grenoble Alpes, LGGE, F-38041 Grenoble, France

³ LOCEAN, CNRS/MNHN/IRD/UPMC, Paris, France

⁴ NOC, Southampton, UK

⁵ Met Office, Exeter, UK

⁶ LOS, IFREMER, Brest, France

* Corresponding author : Nacho Merino, email addresses : ignacio.merino.cue@gmail.com ;
ignacio.merino@lgge.obs.ujf-grenoble.fr

Abstract :

Recent increase in Antarctic freshwater release to the Southern Ocean is suggested to contribute to change in water masses and sea ice. However, climate models differ in their representation of the freshwater sources. Recent improvements in altimetry-based detection of small icebergs and in estimates of the mass loss of Antarctica may help better constrain the values of Antarctic freshwater releases. We propose a model-based seasonal climatology of iceberg melt over the Southern Ocean using state-of-the-art observed glaciological estimates of the Antarctic mass loss. An improved version of a Lagrangian iceberg model is coupled with a global, eddy-permitting ocean/sea ice model and compared to small icebergs observations. Iceberg melt increases sea ice cover, about 10% in annual mean sea ice volume, and decreases sea surface temperature over most of the Southern Ocean, but with distinctive regional patterns. Our results underline the importance of improving the representation of Antarctic freshwater sources. This can be achieved by forcing ocean/sea ice models with a climatological iceberg fresh-water flux.

Highlights

► H1: The Antarctic iceberg freshwater flux is estimated with a sea ice/ocean/iceberg model ► H2: Including vertical profiles of ocean currents improves modelled iceberg trajectories ► H3: The iceberg model overall reproduces the observed probability of iceberg presence. ► H4: Iceberg meltwater increases sea ice formation with few local deviations. ► H5: A climatology of iceberg freshwater flux is offered to be used in climate models

Keywords : Icebergs, Southern Ocean, Sea ice, Freshwater fluxes

List of figures and supplementary files captions

Figure1: Modelled ocean temperatures of the last year of a 20-years ORCA025 simulation coupled with the NEMO-ICB module. (a) Sea Surface Temperature. (b) Averaged temperature over the first 150 m from the surface.

Figure2: 5 Examples of trajectories of modelled icebergs. (a) Trajectories of 73m-thick icebergs of class number 2 with their corresponding sources points (see Supplementary Material); (b) Trajectories of 133m-thick icebergs of class

number 3 and the name of relevant sectors. Red dots correspond to trajectories only considering the drag exerted by the ocean surface, and blue dots correspond to icebergs considering the vertical integrated ocean drag.

Figure3: Sea ice concentration means for: (a) Summer in model results, (b) summer from observations, (c) winter in model results, and (d) winter from observations. Summer means include months from October to March. Winter means includes months from April to September. Model results correspond to ICBT (simulation with explicit icebergs) monthly means of the first 5 years after the 9-year spin up. Observations correspond to the National Snow and Ice Data Center (NSDIC) (Peng et al., 2013) sea ice concentration climatology of the period 1979-2010. Concentrations lower than 10% are not show.

Figure4: Standard deviation of the yearly mean sea ice concentration for the first 5 years after the 9-year spin up of ICBT (simulation with explicit icebergs).

Figure5: Probability of iceberg detection in a 100 km x 100 km grid cell during a year. (a) Observations from ALTIBERG database (Tournadre J., 2015), (b) Model results. Points where annual mean sea ice cover is larger than 40% are shaded.

Figure6: Climatology of iceberg freshwater flux over the Southern Ocean in mm/day for (a) summer, (b) autumn, (c) winter and (d) spring seasons. The flux is computed from 11 years of ICBT (simulation with explicit icebergs) after 9 years of spin-up.

Figure7: Spatial and monthly Integration of the iceberg freshwater fluxes per Southern Ocean sector. Dashed lines correspond to annual means. Red, green, blue and black lines correspond to Atlantic, Indian, Pacific and global sectors respectively

Figure8: (a) Anomalous sea ice concentration in ICBT (simulation with explicit icebergs) versus CTR (simulation without icebergs fluxes).. (b) Anomalous sea ice thickness in ICBT versus CTR.. Results are computed from sea ice monthly means obtained for the first 5 years of simulations after the 9-years spin-up

Figure9: Climatological seasonal cycles of sea ice volume in ICBT (simulation with explicit icebergs) (solid line) and CTR (simulation without icebergs fluxes) (dashed line), for all the Southern Ocean, Atlantic, Pacific, Indian and Bellingshausen Sea sectors respectively.

Figure10: (a) Anomalous sea ice concentration in ICBT (simulation with explicit icebergs) versus CLIM (simulation forced with icebergs fluxes) . (b) Anomalous sea ice thickness in ICBT versus CLIM. Results are computed from sea ice monthly means obtained for the first 5 years of simulations after the 9-years spin-up

Figure11: Mean sea surface temperature difference between ICBT (simulation with explicit icebergs) and CTR (simulation without icebergs fluxes) simulations averaged over January, February and March of the first five years of the simulation after spin-up. This plot shows the cold temperature anomaly in the seasonal ice zone in the Weddell and the warm temperature anomaly west of the Antarctic Peninsula.

Supplementary file Iceberg-Source-Points-Merino.xls: Distribution of iceberg

source points along the model coastline. The table provides the longitude,
55 latitude and calving rate (in Gt/year) corresponding to each iceberg source
point of the iceberg model. Calving rates for each ice-shelf and oceanic sector are
extracted from Depoorter et al. (2013) and distributed along the corresponding
ice-shelf and sector coastline on NEMO ORCA025 grid.

Supplementary file Iceberg-Climatology-Merino.nc : Monthly climatology of
60 iceberg meltwater flux. Monthly means are computed using the last 11 years
of ICBT (simulation without icebergs fluxes) after the spin-up period. The
NetCDF file contains the longitude, the latitude and the freshwater flux for
each grid cell and month.

1. Introduction

65 In contrast with the rapid sea ice loss observed in the Arctic, satellite obser-
vations show a slight overall increase in sea ice extent (SIE) around Antarctica in
recent decades (Comiso and Nishio, 2008; Parkinson and Cavalieri, 2012). The
overall increase in SIE results from the integration of large regional increases
and decreases in sea ice concentration (SIC) around Antarctica (Turner et al.,
70 2009). While the amplitude of overall trend is open to debate, the geographi-
cal pattern of regional changes in SIC has been clearly detected in satellite
observations (Eisenman et al., 2014). The mechanisms driving overall change in
Antarctic sea ice and its regional pattern are also not fully understood as climate
models generally fail to simulate these trends in a rigorous manner (Polvani and
75 Smith, 2013; Gagne et al., 2015; Turner et al., 2015). Whether this is indicative
of a poor representation of physical processes in climate models, for instance
the modelled ice drift (Uotila et al., 2014), or reflects the fact that the observed
trend in SIE results from natural variability is still unclear.

Several model and observational studies have investigated the causes of
80 the increase in Antarctic SIE observed over recent decades. Proposed exter-
nal drivers for such change include winds, air-temperature, precipitation and
freshwater forcing (FWF) from Antarctica. Model experiments show that the
changes in surface winds and air temperature associated with a positive trend
in the Southern Annular Mode contribute to regional changes in Antarctic SIC
85 with a spatial pattern similar to the observed trends (Lefebvre et al., 2004).
The role of changing winds appears to be dominant in the regional response
to changing atmospheric conditions around Antarctica, through a combination
of changes in wind-driven advection of sea ice and wind-driven thermodynamic
changes (Holland and Kwok, 2012; Fan et al., 2014; Holland et al., 2014). How-
90 ever, changes in winds do not appear to quantitatively account for all the changes
observed in SIE (Liu et al., 2004; Fan et al., 2014). Changes in Antarctic SIE
may also involve ice-ocean feedback (Zhang, 2007; Goosse and Zunz, 2014) and
ice-atmosphere feedback (Stammerjohn et al., 2008).

It has also been suggested that the increase in Antarctic SIE may be due in
95 part to changes in freshwater release from the Antarctic Ice sheet (AIS) (Bin-
tanja et al., 2013; Swart and Fyfe, 2013). This hypothesis is consistent with the

observed acceleration of the mass loss from the AIS (Shepherd et al., 2012; Rignot et al., 2008). The oceanic response mechanism involves freshwater-induced changes in ocean surface stratification and convection regimes (Marsland and Wolff, 2001). However, to date, there is no quantitative agreement among existing model studies regarding the impact of the accelerated mass loss from the AIS on Antarctic sea ice. This discrepancy is arguably due to the different and crude representations of freshwater forcing from AIS in ocean models.

The oceanic freshwater forcing from AIS combines the contributions of basal melt in ice-shelf cavities around Antarctica and freshwater fluxes due to melting icebergs over the Southern Ocean. While the input of freshwater due to basal melt occurs at the base of each ice-shelf, icebergs are calved at ice-shelf fronts and melt progressively as they are transported northwards over the Southern Ocean. Reliable estimates of present-day sub ice-shelf melt and calving rates are now available for each ice-shelf (Depoorter et al., 2013; Rignot et al., 2013). However, the redistribution of iceberg mass over the Southern Ocean remains imperfectly constrained, so that ocean model studies differ in their representation of iceberg melt over the Southern Ocean (Bintanja et al., 2013; Swart and Fyfe, 2013; van den Berk and Drijfhout, 2014).

Over the last decade, observations of iceberg distribution and melt rate have mostly been limited to the tracking of large tabular icebergs (i.e. longer than 18km) (Silva et al., 2006). Recent methods based on radar altimetry make it possible to estimate the distribution of the annual mean volume of icebergs and the annual mean melt rates associated with smaller icebergs (up to about 3 km in length) (Tournadre J., 2015). However, accurate estimates of the seasonal and spatial distribution of iceberg melt rates are still not possible because it would require tracking individual icebergs to determine where freshwater release actually occurs. In addition, the altimeter detection of icebergs is limited to sea ice free water and by constraints due to satellite orbits over the southernmost latitudes. Alternatively, explicit iceberg models based on a Lagrangian representation of collections of icebergs have also been proposed as an alternative for estimating freshwater releases from icebergs over the Southern Ocean (Bigg et al., 1997; Gladstone et al., 2001). A widely used climatology of Antarctic iceberg freshwater fluxes, proposed by Silva et al. (2006), combines observations of large tabular icebergs and modelling of small icebergs.

Several Lagrangian iceberg models have recently been coupled with ocean circulation models at various grid resolutions (Martin and Adcroft, 2010; Jongma et al., 2009; Marsh et al., 2015). These models, however, do not yet use the most up-to-date estimates of calving rates (Depoorter et al., 2013; Rignot et al., 2013). Moreover, modelled iceberg distributions have not yet been systematically compared with observations from radar altimetry. Tournadre et al. (2012) also suggest that existing models might not be able to adequately represent iceberg trajectories across Southern Ocean subpolar gyres (especially in the Weddell Gyre). This may be due to biases in current Lagrangian iceberg models, which are driven by ocean surface fields, or to the coarse resolution of most ocean circulation models coupled with iceberg models.

In this paper, we propose a model-based estimate of iceberg melt over the

Southern Ocean and study the impact of iceberg melt on ocean surface properties and sea ice. The estimate is obtained with an improved version of a Lagrangian iceberg model coupled with an eddy-permitting ocean-sea ice model, using the most recent input calving rates based on glaciological studies. The modelled iceberg distribution is shown to compare favourably with observations in most of the Southern Ocean sectors. We show the strong seasonality of iceberg freshwater releases over the Southern Ocean and discuss its impact on Antarctic sea ice. We further show that the impact of icebergs on Antarctic sea ice can be reproduced, to a large extent, by forcing the ocean-sea ice model with a climatological iceberg freshwater flux (provided as Supplementary Material). The methods are described in section 2. The modelled distribution of icebergs is presented and compared with observations in section 3. The impact of iceberg freshwater release on sea ice is discussed in section 4. Finally, section 5 draws conclusions and discusses the proposed climatology of iceberg freshwater fluxes.

2. Material and methods

The distribution of freshwater fluxes due to icebergs is estimated here with an interactive ocean/sea ice/iceberg model forced with recent estimates of Antarctic freshwater forcing. In this section we describe the details of the model set up and the different datasets used to perform this work.

2.1. Ocean/sea ice model configuration

The ocean simulation is based on NEMO v 3.5 (Madec, 2014). The model configuration uses a 0.25-degree resolution grid (ORCA025) with 75 vertical levels developed and maintained by the DRAKKAR group. Ice-shelf cavities are not explicitly represented in the model, but ice-shelf meltwater is prescribed (see section 2.3). The ocean component is coupled with the LIM2 sea ice model (Fichefet and Morales Maqueda, 1997) and the NEMO iceberg module (Marsh et al., 2015) (see section 2.2). The ocean model is forced by using core bulk formulae with a climatological repeated-year atmospheric forcing based on ERA-Interim (Dee et al., 2011). The climatological repeated-year forcing is constructed following the same approach as Grégorio et al. (2015) itself based on Penduff et al. (2011). This forcing is built by computing 365 ERA-Interim daily averages for the period 1979-2011. The resulting atmospheric forcing is composed of the daily averages of precipitations, runoff, cloud cover, long and short wave radiation, 10 meters winds, temperature and air humidity. In addition quadratic contributions are added to air-sea fluxes in order to account for the contribution of non-linear high frequency correlations in bulk formulae. A sea surface salinity restoring towards NODC WOA94 data, with a piston velocity (Griffies et al., 2009) of 50 m/300 days, is applied, except at the first coastal grid points. This is commonly practised in stand-alone ocean/sea ice DRAKKAR simulations in order to not affect the total coastal runoff in the simulations.

2.2. Standard NEMO-ICB and new features in NEMO-ICB

The ocean component is coupled with the NEMO-ICB iceberg module (Marsh et al., 2015). It describes the evolution of an ensemble of Lagrangian particles. Each Lagrangian particle is meant to represent a collection of one or several icebergs. Each collection of icebergs belongs to one of the ten different size categories of the statistical distribution based on ship observations proposed by Gladstone et al. (2001). By simplicity, a constant upper bound of 250 m is considered for all the ice shelves in this study, consistently with Martin and Adcroft (2010) and Marsh et al. (2015). This upper bound corresponds to the typical thickness of ice-shelves at their calving front. NEMO-ICB considers a fixed number of source points with constant in time iceberg production rate for each individual source location. The dynamics and thermodynamics of each collection of icebergs are prescribed according to the procedure used by Marsh et al. (2015), which mostly follows Martin and Adcroft (2010). Freshwater fluxes to the ocean model are calculated at each time-step from the iceberg melt rate and injected at the ocean surface. However, in the present version of NEMO-ICB, heat fluxes from icebergs are not applied to the ocean model: neither sensible heat fluxes due to iceberg-ocean temperature difference, nor latent heat of fusion when melting are taken into account.

As is common in iceberg models, the model only describes the evolution of small icebergs (up to 2.2km in length). This choice is supported by the findings of Tournadre et al. (2015) indicating that the melting of large icebergs provides only a marginal contribution to total iceberg freshwater fluxes.

2.2.1. NEMO-ICB module modifications

Unlike previous versions of Lagrangian iceberg models (Bigg et al., 1997; Gladstone et al., 2001; Martin and Adcroft, 2010), the model used here (NEMO-ICB module, including the modifications described in section 4 of Marsh et al., 2015) takes into account the influence of the vertical profiles of ocean currents and temperatures instead of only considering the SST and surface ocean velocities, and considers a parametrised interaction with shallow bathymetry. Those modifications (firstly implemented for this work) are described in this section and are found to significantly improve the representation of iceberg trajectories across Southern Ocean subpolar gyres (see section 2.2.2).

The first modification introduced in NEMO-ICB is the vertical integration of ocean currents that takes into account the drag exerted by the entire ocean column in contact with the iceberg, instead of the drag exerted by the ocean surface. This modification allows in particular to take into account the change in the orientation of wind driven currents with depth in the Ekman layer, which is approximately 100 m deep in the Southern Ocean (Lenn and Chereskin, 2009).

The second modification is the computation of melt rates using ocean temperatures at varying depths, thus taking into account the strong vertical temperature gradients in summer in the upper Southern Ocean. Modelled icebergs, according to observations, can be up to 250 m thick (Gladstone et al., 2001) and the ocean temperature profiles across the pycnocline in summer can be remark-

ably abrupt in shallow mixed layers. As shown in Figure 1, surface temperatures and first depth averaged temperatures over 0-150m can differ significantly in some regions.

230 The last modification introduced in this work is the parametrization of iceberg interaction with bathymetry. With the inclusion of the vertical integration of the ocean currents, the interaction of thick icebergs with shallow bathymetry needs to be explicitly taken into account. This is because, accounting for the ocean drag is needed when a thick iceberg crosses a shallow bathymetry grid
235 cell. We choose not to stop icebergs in shallow regions because the subgrid scale bathymetry probably matters more than the model bathymetry. Nonetheless, we calculate the vertically-averaged velocity over the entire iceberg thickness, with zero velocities at depth where the iceberg is deeper than the model bathymetry, so icebergs are slowed in shallow regions (see equation 1 in Appendix).
240 By including this interaction in the model, thick icebergs tend to stay longer in specific coastal regions instead of escaping northwards as it happened in previous versions of the iceberg model. This overall behaviour is in better agreement with observations which indicate the existence of regions with high iceberg presence due to the grounding of thick ones (Jacka and Giles, 2007).

245 *2.2.2. Impact of vertical shear on simulated iceberg trajectories*

As described in section 2.2.1 the iceberg model used in this study considers ocean currents averaged over the thickness of each iceberg in the drag formulation, instead of the ocean surface currents as commonly applied in previous iceberg modelling studies.

250 Figure 2 shows the sensitivity to this modification for individual iceberg trajectories departing from different locations and for two different size classes. Icebergs of category #1 and #2 (40m and 67m thickness respectively, Gladstone et al. (2001)) are thinner than the typical thickness of the Ekman layer and are therefore not significantly affected by the modification in NEMO-ICB (Figure
255 2a). By contrast, larger and thicker icebergs can only cross the Weddell, Ross, and Amery Seas if the vertical integration of ocean velocities is included in NEMO-ICB (Figure 2b). Icebergs following the Antarctic Coastal Current are more likely to escape before reaching the Antarctic Peninsula and to the north of the Weddell Sea. Consequently, our modification leads to a reduced presence
260 of modelled icebergs in the Atlantic sector, and contributes to better distribute the iceberg mass between Atlantic, Indian and Pacific sectors.

2.3. Observation-based calving and meltwater input fluxes

265 The recent estimate of Antarctic freshwater forcing from Depoorter et al. (2013) is used in our simulations. Depoorter et al. (2013) provide calving rates and basal melt fluxes for 31 ice-shelves around Antarctica. The total observed mass loss from Antarctica is completed with an additional residual flux for each Southern Ocean sector. Both the calving rates and the basal melt rates are in good agreement with another recent observational study (Rignot et al., 2013).

270 These recent estimates provide a major improvement over the Antarctic freshwater forcings used in previous studies (eg. van den Berk and Drijfhout,

2014). Indeed, the most recent estimates (Depoorter et al., 2013; Rignot et al., 2013) account for the observed changes in ice-shelf thickness and surface mass balance, in contrast with earlier studies (eg. Rignot and Jacobs, 2002). In addition, improved techniques for grounding line detection, thickness measurements and firn model corrections have been applied to the treatment of the most recent data (between 1994 and 2009) (Depoorter et al., 2013).

Basal melt underneath ice-shelves is prescribed as coastal run-off in our simulation set-up. Following Depoorter et al. (2013), it accounts for 1454 Gt/yr and is distributed at the ice-shelf fronts. The corresponding freshwater flux is applied at ocean grid points lying at the front of each ice-shelf and spread vertically between the base of the calving front and the minimum between the grounding line depth and the bathymetry at the calving front. The 1350 Gt/yr of calving fluxes estimated in Depoorter et al. (2013) are used as input for the NEMO-ICB module. The iceberg model then generates icebergs, which eventually distribute freshwater at the ocean surface when they melt. Calving rates are kept constant over time and their spatial distribution follows Depoorter et al. (2013). The distribution of source points for iceberg calving is provided in Supplementary Material.

2.4. Model experiments

Three experiments based on the described model set up have been run in this work. The *iceberg test run* (hereafter referred to as ICBT) uses the ocean/sea ice model configuration coupled with the iceberg model described above in section 2.2 in a 20-year simulation. The ICBT simulation initial state is free of icebergs. The first 9 years of ICBT simulation correspond to the spin-up required for the iceberg model. In steady state after the spin-up, the calving mass input matches the melted iceberg mass. In contrast, in the *control run* (hereafter CTR), the iceberg model is switched off, and consequently, the ocean/sea ice model does not include any flux from icebergs. CTR is computed for 14 years, that correspond to 9 years of spin-up and 5 years for results comparison with ICBT results. Considering the constant climatological atmospheric forcing applied, the reduced ocean/sea ice model variability allows 5-years means comparisons between both simulations. An extra simulation of 14 years (hereafter CLIM) was performed without the iceberg model but including, as an external forcing, a monthly climatology of iceberg freshwater flux. This climatology (available in Supplementary Material) has been computed from the monthly means of the ICBT simulation (see section 4.1)

3. Model evaluation

3.1. Ocean/sea ice model

Figure 3 shows the comparison of the modelled sea ice with observations. Modelled SIC is computed from monthly means of ICBT simulation after spin-up. Observations of sea ice concentration come from NSDIC monthly means for the period 1979-2010. Summer means includes the months from October

to March, and winter means include months from April to September. ICBT simulation presents more sea ice concentration than observations in the Belling-
 315 shausen Sea in both summer and winter seasons. In summer, sea ice concentration gradients are overall stronger in the model. Besides, simulated summer sea ice is more concentrated in coastal regions of the Atlantic and East Indian sectors and less concentrated in Ross Sea.

The choice of comparing 5-years sea ice means between the different simulations (see section 2.4) is supported by the Figure 4. It shows the standard
 320 deviation of the sea ice concentration for the 5-year period after the 9-years spin-up of the ICBT simulation. As shown in Figure 4, the inter annual variability of the sea ice for ICBT simulation is mostly negligible. Large standard deviations are obtained near sea ice margins where year to year variability in
 325 SIC is expected to be large.

3.2. Iceberg model

3.2.1. On the model-observations comparison of iceberg presence

Iceberg model results are compared to ALTIBERG database (Tournadre J., 2015). This database uses the method described in Tournadre et al. (2012)
 330 applied to Jason-I and 9 other satellites covering various time periods from 1992 to 2014. The database provides a single estimate of iceberg volume per grid cell for icebergs of 0.1 to 3 km in length. It is based on the assumption of a constant iceberg thickness of 247 m. Our study divides this volume by the thickness (247 m) to obtain the area covered by icebergs in each grid cell.
 335 Taking into account grid cell area, we can compute the ratio between the surface covered by icebergs and the ocean surface. This can also be understood as the probability of detecting an iceberg of 0.1 to 3 km in length in a grid cell. A similar estimation can be made from model results. The total area covered by modelled icebergs is integrated over the same grid as the observations and
 340 averaged over a year.

Satellite detection of icebergs with radar altimetry is limited by the presence of sea ice. Icebergs can only be detected in sea ice free water and the comparison in regions with high annual sea ice concentration needs to be carefully considered. In order to highlight those sectors, we decided to mask in Figure 5 the
 345 regions with sea ice concentration greater than 40%, consistently with the ALTIBERG data treatment. We use observations of mean sea ice cover provided by the NSIDC (Peng et al., 2013) instead of our modelled sea ice concentrations, so as to be more consistent with ALTIBERG detections.

The quantitative comparison of modelled and observed icebergs should be
 350 considered with caution because of the specificities of iceberg detections and model settings. On the observation side, the method of Tournadre et al. (2012) only detects small icebergs of up to 3 km in length. Therefore a significant fraction of the total volume of icebergs, corresponding to icebergs longer than 3 km, is not directly observed with radar altimetry. On the model side, the
 355 distribution of iceberg class sizes, which follows Gladstone et al. (2001), assumes that the total annual volume of icebergs is distributed in iceberg classes of up to

2.2km in length. Given that the thickness of icebergs depends on the category, the model probably overestimates the area covered by small icebergs.

3.2.2. Qualitative model-observations comparison

360 Figure 5 compares the iceberg distribution in the model with observations from the ALTIBERG database (Tournadre J., 2015). It shows the probability of detecting an iceberg in a grid cell of 100 km x 100 km over a year following the method described in section 3.2.1. To our knowledge, this is the first qualitative comparison between an iceberg model and the distribution of small icebergs
365 estimated from radar altimetry observations. Patterns of the probability of iceberg presence is overall well reproduced by the model. Indeed, the model correctly computes highly probability of finding icebergs in offshore branches of Antarctic subpolar gyres. The model also reproduces the observed pattern of iceberg presence in the eastward flowing branch of the Weddell Gyre. This
370 pattern is consistent with the observations of Tournadre et al. (2012) (see their Figure 16), whereas most existing iceberg models show major discrepancies in this region (Tournadre et al., 2012). As shown in Figure 6, the presence of icebergs in this region significantly increases the freshwater flux in the Atlantic sector of the Southern Ocean. The improved distribution of icebergs in this
375 region compared with previous studies is likely due to the depth integration of ocean currents as discussed in section 2.2.2.

Several differences between the model and observations can also be identified. First, the model suggests a higher probability of iceberg presence in coastal regions compared with observations. It should be noted that most of the iceberg
380 detections in those coastal sectors have been dismissed from ALTIBERG database based on their sea ice criteria (Tournadre J., 2015). However, synthetic aperture radar images (Wesche and Dierking, 2015) confirm the high presence of small and medium size icebergs trapped in the Antarctic Coastal Current in the Indian and Atlantic sectors. Second, in the model, the Weddell Sea sector
385 presents a relatively larger iceberg-covered area than that found in the Amery or Ross sectors, whereas observations indicate roughly similar probabilities of iceberg presence in all three Antarctic subpolar gyres. This might indicate that the modelled icebergs are too often trapped within the Antarctic Coastal Current. Indeed, the Antarctic Peninsula is the last escape route for icebergs transiting
390 along the Antarctic Coastal Current. Model misrepresentation of the ability of icebergs to escape coastal regions would therefore result in an increase in iceberg presence north of Weddell Sea. This happens even if, as shown in section 2.2.2, modifications of the iceberg model used in this study tend to decrease the number of icebergs that eventually reach the Antarctic Peninsula. A further
395 misrepresentation of escape routes from coastal regions in the model could also be associated with the representation of iceberg interaction with sea ice, firstly suggested by Lichey and Hellmer (2001), proposed by Hunke and Comeau (2011) and observed by Schodlok et al. (2006). In addition, mesoscale variability in the Antarctic Coastal Current is significant (Stewart and Thompson, 2015),
400 but probably too weak in the model, which may contribute to limit the escape of modelled icebergs from coastal regions. The model also shows a lack of icebergs

in open ocean waters of the South-East Pacific sector. This could be related to the fact that the model only considers coastal sources of icebergs, whereas observations suggest that large icebergs, which are not represented in the model, break into small icebergs in open ocean waters (Tournadre et al., 2015). These resulting smaller icebergs are then transported by the ACC and reach the west Antarctic Peninsula and the South Atlantic sectors before melting. Neglecting the formation of small icebergs associated with the breaking of large ones is therefore likely to contribute to discrepancies in the South-East Pacific and in the South Atlantic.

4. Results

4.1. Iceberg freshwater flux climatology

Starting from an initial state free of icebergs, the iceberg model takes about 9 years to reach equilibrium, when iceberg melt water balances the calving flux. At model equilibrium in ICBT run, the Southern Ocean presents a yearly mean iceberg mass close to 3000 Gt, more than twice the iceberg mass input and the melted mass released over one year. This indicates that, on average, model icebergs are transported for more than one year before melting. We find in particular that icebergs usually follow the Antarctic Coastal Current for more than one year before reaching the open ocean. This is also consistent with recent estimates of the volume of icebergs near the coast of Antarctica (Wesche and Dierking, 2015). Icebergs eventually leave coastal regions carried by offshore flows associated with the three Antarctic subpolar gyres in the Weddell, Ross and Amery sectors (see Figure 5). Such iceberg behaviour in the model is consistent with satellite observations (Tournadre et al., 2012) and was previously reported in the eastern Weddell Sea by Schodlok et al. (2006).

The 11-years climatological estimate of iceberg freshwater release over the Southern Ocean are shown in Figures 6 and 7. This estimate confirms that iceberg melt over the Southern Ocean is very heterogeneous. For instance, since most of the iceberg mass is concentrated in the Weddell Sea sector, this is where most of the freshwater release occurs. In contrast, iceberg freshwater release appears to be relatively limited in the Bellingshausen Sea, west of the Antarctic Peninsula, most probably because this region is not fed by icebergs flowing from upstream sources along the Antarctic Coastal Current. Our estimate also confirms that iceberg melt exhibits strong seasonality over the Southern Ocean, as suggested by Tournadre et al. (2012) and shown in Figure 7. The freshwater flux is indeed usually below the annual mean value for more than two thirds of the year, with about 43% of annual fresh-water release occurring from December to February. The strongest seasonality is observed in the Ross Sea and Amundsen Sea sectors in the Pacific, where January and February account for almost half of the net annual freshwater flux. Surprisingly, the seasonality of the freshwater flux in the Indian sector is slightly delayed as compared to other regions, with a maximum flux occurring in February and relatively weak fluxes in December and January.

445 4.2. Sensitivity of sea ice to icebergs

Figure 8 shows the differences in annual mean sea ice concentration and thickness for ICBT and CTR simulations. It considers the first 5 years after the 9 years of spin up. It reveals that the freshwater release due to icebergs increases sea ice concentration and thickness over most of the Southern Ocean with the exception of the Bellingshausen Sea. Those results are discussed in section 5. The sea ice volume seasonal cycles of both ICBT and CTR simulations are compared in Figure 9. As shown in Figure 9, both simulations present a very similar minimum of sea ice volume with remarkable differences in their maximum in most of the Southern Ocean sectors. In addition, there is no shift between the sea ice cycle of both simulations, so the maximum and the minimum happen at the same time of the year for all the analysed sectors. Overall, iceberg freshwater release therefore increases the amplitude of the seasonal cycle of sea ice with larger net production and sea ice melting. These changes lead to an increase of 10% in the annual mean sea ice volume. However, in terms of relative quantities, the largest relative global difference between ICBT and CTR occurs in mid-April, at the beginning of the sea ice production period, with a 14.3% larger sea ice volume with icebergs (ICBT). In summer, when sea ice volume is at a minimum, it is 10% larger with icebergs (sea ice extent is 13.5% larger). In winter, when sea ice volume reaches a maximum, it is 8.3% larger with icebergs (sea ice extent is only 2.5% larger). Overall, iceberg freshwater release therefore increases the amplitude of the seasonal cycle of sea ice volume with larger net production and the melting of sea ice.

The CLIM experiment (see section 2.4) was performed to study the ability of the ocean model to account for the iceberg freshwater fluxes with a reduced CPU cost as compared to ICBT simulation. For instance, the first year after spin-up takes 47% less CPU time for CLIM than for ICBT. Figure 10 shows the difference in annual mean sea ice concentration and thickness for ICBT and CLIM simulations. It considers the first 5 years after 9 years of spin up. This result reveals strong similarities in the solution obtained when an external forcing is applied at the ocean surface instead of explicitly solving the icebergs dynamics and thermodynamics. This result shows that most of the impact on the sea ice can be captured with the inexpensive approach applied for the CLIM simulation. Differences obtained in most of the Southern Ocean are indeed negligible compared to the differences between ICBT and CTR simulations (see Figure 8).

5. Discussion of the impact of icebergs on sea ice and ocean surface

Freshwater fluxes at the ocean surface directly affect surface salinity, ocean stratification and mixed layer depth through changes in bouyancy fluxes at the ocean surface. These changes in surface properties can also indirectly affect sea surface temperature (SST) and sea ice cover (as it is shown in section 4.2). Two important mechanisms can be expected to play a role in the response of Antarctic sea ice to iceberg freshwater release. Firstly, during fall and winter months, when the atmosphere extracts heat from the ocean, a freshening

of ocean surfaces enhances thermohaline stratification, thereby weakening the
490 rate of convective overturning and therefore the supply of heat to the surface
layers from deeper layers. This leads to an increase in net sea ice production
because the heat supply from the deep ocean no longer limits sea ice production
(Marsland and Wolff, 2001). Secondly, a freshening of the ocean surface also
495 contributes to create shallower mixed layers, thus decreasing the effective heat
capacity of ocean surface layers. Ocean surface layers are then more sensitive
to air-sea heat fluxes. Under a positive air-sea downward heat flux (e.g. during
the melting season), the ocean surface receives more heat, thereby accelerat-
ing sea ice melt. Increased sea ice production with icebergs over most of the
Southern Ocean is consistent with the mechanism involving the reduction of
500 convective overturning in winter described by Marsland and Wolff (2001). For
instance, iceberg freshwater release significantly reduces convective overturning
in the Weddell Sea, delaying the seasonal opening of Maud Rise Polynia and
increasing annual mean sea ice cover in this region. In addition, the model
indicates that summer mixed layers (not shown) are shallower with icebergs,
505 consistently with a reduction in the effective heat capacity of ocean surface lay-
ers. One could expect that the reduction in heat capacity in ICBT simulation
would drive a surface warming during summer as compared to CTR simulation.
On the contrary, model SST in the seasonal ice zone are usually considerably
colder ($0.5-1^{\circ}\text{C}$) with icebergs (see Figure 11). This is probably related to the
510 difference in winter sea ice concentration and thickness between ICBT and CTR.
Changes in winter sea ice concentration and thickness may cool the SST by two
mechanisms: Firstly, the extra insulation exerted by the thicker or more concen-
trated sea ice layer may reduce the net heat flux received by the ocean surface
layer in spring and summer. Secondly, larger latent heat fluxes are required to
515 melt the extra sea ice volume of the ICBT simulation. Both mechanisms seem
to notably compensate the effect of changes in heat capacity.

As noted above, modelled iceberg melt is relatively limited in the Belling-
shausen Sea west of the Antarctic Peninsula, but the response of the modelled
sea ice to this extra freshwater is significant and somewhat unexpected. In con-
520 trast with most of the Southern Ocean, sea ice tends to be thinner with icebergs
in this region while sea ice concentration is essentially unchanged (see Figure
8). In addition, SSTs are found to be significantly warmer in summer upstream
of the Bellingshausen Sea along the Antarctic Peninsula (see Figure 11). This
suggests that the equilibrium state reached after spin-up in the Bellingshausen
525 Sea may be affected by changes in heat transport by the Antarctic Coastal Cur-
rent. In the model, the lateral supply of warmer water may affect the formation
of sea ice in the Bellingshausen Sea so that the ocean/sea ice system eventually
reaches an equilibrium state with thinner sea ice over the entire annual cycle.
What drives the warming of surface layers upstream is not clear yet, but this
530 warming could be associated with changes in effective heat capacity of ocean
surface layers in coastal regions along the Antarctic Peninsula. Other processes
in the model, as for instance changes in the convective supply of heat to the
surface could also contribute to the unexpected response of simulated sea ice
properties in the Bellingshausen Sea. But further analysis would be needed to

535 disentangle the mechanisms involved. In conclusion, the response in terms of
modelled sea ice volume in the Bellingshausen Sea illustrates how icebergs can
affect ocean surface properties through a range of physical processes. Indeed,
the Bellingshausen sector presents the only discrepancies between ICBT and
CLIM simulations (see Figure 10). The forced simulation (CLIM) produces
540 even thinner sea ice than ICBT and CTR. The three simulations notably differ
in their sea ice thickness solution in the Bellingshausen sector. However, the
icebergs fluxes in the sector seems to be weaker than what the observations sug-
gests (see Figure 5), and the discussed mechanism producing sea ice thinning
should not be considered as a realistic climate feature in the sector. Instead,
545 the Bellingshausen Sea in the model is an example which illustrates how, under
specific conditions, the way icebergs fluxes are represented in the ocean models
may be crucial to model sea ice.

6. Conclusions

In this paper, we have studied the climatological distribution of iceberg melt
550 over the Southern Ocean and its impact on Antarctic sea ice and ocean surface
properties. To do this, we have used a Lagrangian iceberg model (Marsh et al.,
2015) coupled with a global, eddy-permitting ocean sea ice model configuration
(NEMO-ORCA025). The Lagrangian iceberg model has been modified in order
to explicitly take into account the influence of ocean current and temperature
555 vertical profiles. Ocean currents integrated along the iceberg vertical profile are
shown to notably impact the trajectories of icebergs crossing the subpolar gyres
in the Ross, Amery and Weddell Seas. The model is forced with recent estimates
of calving rates and melt rates for the Antarctica Ice Sheet (Depoorter et al.,
2013).

560 The distribution of Antarctic icebergs in the model is shown to be broadly
consistent with satellite observations of small icebergs from radar altimetry. We
have presented the first comparison of the probability of iceberg detection ob-
tained from radar altimetry with that from an iceberg model. This comparison
makes it possible to identify limitations of current Lagrangian iceberg models

565 For instance, modelled icebergs seem to be too confined in the Antarctic
Counter Current, which impacts the equatorward transport of icebergs through
the Ross and Amery subpolar gyres. In addition, modelled iceberg trajectories
seem too short in the model, especially in the Pacific sector where observations
suggest that icebergs are transported further east. Improving the representation
570 of icebergs/sea ice interaction may also improve simulation results, either by
producing more export of icebergs out of the Antarctic Counter Current follow-
ing the drift of the sea ice pack, or by fastening iceberg close to coast within
fast sea ice. Additionally, a higher ocean model resolution and the representa-
tion of the synoptic component of the wind forcing could help icebergs escaping
575 the Antarctic Counter Current. Finally, accounting for small icebergs associ-
ated with the fracturing of large tabular, could result in trajectories extending
further east and might lead to a better agreement between the model and the

altimetry observations. This could be reproduced in the model by adding off-shore calving sources in the model according to a probabilistic estimation of the tabular iceberg fracturing.

Iceberg melt over the Southern Ocean is found to show a significant seasonality and to be mostly concentrated in offshore flowing branches of Antarctic subpolar gyres. A large fraction of the total iceberg melt is found to occur in the South Atlantic sector of the Southern Ocean. The freshwater release is found to be strongly seasonal in the Ross Sea and the Amundsen Sea where almost half of the freshwater release occurs in January and February. The monthly climatology of iceberg melt over the Southern Ocean is provided as Supplementary Material.

Iceberg melt is shown to substantially increase sea ice concentration and thickness over most of the Southern Ocean, except in the Bellingshausen Sea where iceberg melt decreases sea ice thickness in the model. As suggested by previous studies, in most of the Southern Ocean, iceberg melt increases sea ice production in autumn and winter because it reduces convective overturning, thus limiting the heat supply from the deep ocean to the surface. In contrast, iceberg melt results in thinner sea ice in the Bellingshausen Sea, probably because of the advection of warmer waters flowing along the Antarctic Coastal Current.

The extra computational cost of running an explicit iceberg model can be drastically reduced by forcing the ocean model with a monthly climatology of iceberg melt. Figure 10 shows that this inexpensive simulation strategy succeeds in capturing the essential aspects of the response of sea ice to freshwater release in a climatological forced ocean simulation. Whether this result still holds with an inter-annually varying atmospheric forcing needs to be further investigated. Such a forcing strategy could arguably be adopted for forced ocean simulations and possibly adapted to climate models. For climate simulations, latent heat exchanges due to iceberg melt would need to be recalculated from the freshwater fluxes in order for the model to conserve energy.

Appendix: Modified equations of the NEMO-ICB Lagrangian iceberg model

Interested reader may refer to Martin and Adcroft (2010) for a thorough description of the dynamics and thermodynamics of the iceberg model. We only describe here our modifications and the corresponding changes in the original model equations.

The parametrized dynamics of the iceberg model from Martin and Adcroft (2010) which are based on Bigg et al. (1997), depend on the sea surface velocity. In this work we consider the following depth-integrated ocean velocity:

$$\vec{v}_m = \frac{\int_{-\min(H_{bat}, H_{icb})}^0 \vec{v}_o(h) dh}{H_{icb}} \quad (1)$$

where H_{bat} is the bathymetry depth at the grid point, H_{icb} is the submerged part of the iceberg thickness, dh is the differential of depth, $\vec{v}_o(h)$ is the ocean

velocity depending on the depth and $\vec{v}_m(h)$ is the resulting depth-integrated ocean velocity.

620 Our version of NEMO-ICB model uses the equations A.2a A.2b and A.2c from Martin and Adcroft (2010) applying $\vec{v}_m(h)$ instead of the sea surface velocity.

We also modify the equations of the parametrization of basal turbulence and buoyant convection melt rates (see equations A.7 and A.9 from Martin and
625 Adcroft (2010)) as follows:

$$M_b = 0.58|\vec{v} - \vec{v}_b|^{0.8} \frac{\tilde{T}_b - \tilde{T}}{L^{0.2}} \quad (2)$$

with $\vec{v}_b = \vec{v}_{bat}$ and $\tilde{T}_b = \tilde{T}_{bat}$ whenever $H_{icb} > H_{bat}$, where \vec{v} is the iceberg velocity, \vec{v}_b is the velocity of the ocean at the base of the iceberg, \vec{v}_{bat} is the bottom ocean velocity (i.e. at sea floor depth), \tilde{T}_b is the ocean temperature at the base of the iceberg, \tilde{T}_{bat} is the bottom ocean temperature, L is the iceberg
630 horizontal length, and M_b is the resulting basal turbulence melt rate.

Finally, the buoyant convection melt rate is integrated over the depth of the iceberg as follows:

$$M_v = \int_{-H_{icb}}^0 (7.62 \times 10^{-3} \tilde{T}_o(h) + 1.29 \times 10^{-3} \tilde{T}_o^2(h)) dh \quad (3)$$

with $\tilde{T}_o(h) = \tilde{T}_{bat}$ whenever $h > H_{bat}$, where $\tilde{T}_o(h)$ is the ocean temperature at depth h and M_v is the resulting buoyant convection melt rate.

635 7. Acknowledgments

We would like to thank Jean Marc Molines for his invaluable help with model configuration. Numerical simulations were performed on IDRIS supercomputers (Saclay, France). The study was partially funded by the French National Research Agency (ANR) under the SUMER (Blanc SIMI 6) 2012 project, referenced as ANR-12-BS06-0018. NCJ is an Associate Investigator with the AR-
640 CCSS (ARC Centre of Excellence for Climate System Science). **Finally, we would like to thank the three anonymous reviewers and the editor Stephen Griffies for their helpful and constructive contribution to this work.**

References

645 Bigg, G. R., Wadley, M. R., Stevens, D. P., Johnson, J. A., 1997. Modelling the dynamics and thermodynamics of icebergs. *Cold Regions Science and Technology* 26 (2), 113–135.

Bintanja, R., Van Oldenborgh, G., Drijfhout, S., Wouters, B., Katsman, C., 2013. Important role for ocean warming and increased ice-shelf melt in antarctic sea-ice expansion. *Nature Geoscience* 6 (5), 376–379.
650

- Comiso, J. C., Nishio, F., Feb. 2008. Trends in the sea-ice cover using enhanced and compatible AMSR-E, SSM/I, and SMMR data. *Journal of Geophysical Research: Oceans* 113 (C2), C02S07.
 URL <http://onlinelibrary.wiley.com/biblioplanets.gate.inist.fr/doi/10.1029/2007JC004257/abstract>
 655
- Dee, D. P., Uppala, S. M., Simmons, A. J., Berrisford, P., Poli, P., Kobayashi, S., Andrae, U., Balmaseda, M. A., Balsamo, G., Bauer, P., Bechtold, P., Beljaars, A. C. M., van de Berg, L., Bidlot, J., Bormann, N., Delsol, C., Dragani, R., Fuentes, M., Geer, A. J., Haimberger, L., Healy, S. B., Hersbach, H., Hlm, E. V., Isaksen, L., Killberg, P., Khler, M., Matricardi, M., McNally, A. P., Monge-Sanz, B. M., Morcrette, J.-J., Park, B.-K., Peubey, C., de Rosnay, P., Tavolato, C., Thpaut, J.-N., Vitart, F., Apr. 2011. The ERA-Interim reanalysis: configuration and performance of the data assimilation system. *Quarterly Journal of the Royal Meteorological Society* 137 (656), 553–597.
 660
 URL <http://doi.wiley.com/10.1002/qj.828>
- Depoorter, M., Bamber, J., Griggs, J., Lenaerts, J., Ligtenberg, S., van den Broeke, M., Moholdt, G., 2013. Calving fluxes and basal melt rates of antarctic ice-shelves. *Nature*.
- Eisenman, I., Meier, W. N., Norris, J. R., Jul. 2014. A spurious jump in the satellite record: has Antarctic sea-ice expansion been overestimated? *The Cryosphere* 8 (4), 1289–1296.
 670
 URL <http://www.the-cryosphere.net/8/1289/2014/>
- Fan, T., Deser, C., Schneider, D. P., 2014. Recent antarctic sea-ice trends in the context of southern ocean surface climate variations since 1950. *Geophysical Research Letters* 41 (7), 2419–2426.
 675
- Fichefet, T., Morales Maqueda, M. A. M., Jun. 1997. Sensitivity of a global sea-ice model to the treatment of ice thermodynamics and dynamics. *Journal of Geophysical Research: Oceans* 102 (C6), 12609–12646.
 URL <http://onlinelibrary.wiley.com/biblioplanets.gate.inist.fr/doi/10.1029/97JC00480/abstract>
 680
- Gagne, M.-E., Gillett, N. P., Fyfe, J. C., Jan. 2015. Observed and simulated changes in Antarctic sea-ice extent over the past 50 years. *Geophysical Research Letters* 42 (1), 2014GL062231.
 685
 URL <http://onlinelibrary.wiley.com/biblioplanets.gate.inist.fr/doi/10.1002/2014GL062231/abstract>
- Gladstone, R. M., Bigg, G. R., Nicholls, K. W., 2001. Iceberg trajectory modeling and meltwater injection in the southern ocean. *Journal of Geophysical Research: Oceans* (1978–2012) 106 (C9), 19903–19915.
- Goosse, H., Zunz, V., Mar. 2014. Decadal trends in the Antarctic sea-ice extent ultimately controlled by iceocean feedback. *The Cryosphere* 8 (2), 453–470.
 690
 URL <http://www.the-cryosphere.net/8/453/2014/>

- Grégorio, S., Penduff, T., Sérazin, G., Molines, J.-M., Barnier, B., Hirschi, J.,
2015. Intrinsic variability of the atlantic meridional overturning circulation at
interannual-to-multidecadal time scales. *Journal of Physical Oceanography*
45 (7), 1929–1946.
- Griffies, S. M., Biastoch, A., Böning, C., Bryan, F., Danabasoglu, G., Chas-
signet, E. P., England, M. H., Gerdes, R., Haak, H., Hallberg, R. W., et al.,
2009. Coordinated ocean-ice reference experiments (cores). *Ocean Modelling*
26 (1), 1–46.
- Holland, P. R., Bruneau, N., Enright, C., Losch, M., Kurtz, N. T., Kwok,
R., 2014. Modeled trends in antarctic sea-ice thickness. *Journal of Climate*
27 (10), 3784–3801.
- Holland, P. R., Kwok, R., Dec. 2012. Wind-driven trends in Antarctic sea-ice
drift. *Nature Geoscience* 5 (12), 872–875.
URL [http://www.nature.com/biblioplanets.gate.inist.fr/ngeo/
journal/v5/n12/full/ngeo1627.html](http://www.nature.com/biblioplanets.gate.inist.fr/ngeo/journal/v5/n12/full/ngeo1627.html)
- Hunke, E. C., Comeau, D., 2011. Sea-ice and iceberg dynamic interaction. *Jour-
nal of Geophysical Research: Oceans (1978–2012)* 116 (C5).
- Jacka, T. H., Giles, A. B., 2007. Antarctic iceberg distribution and dissolution
from ship-based observations. *Journal of Glaciology* 53 (182), 341–356.
- Jongma, J. I., Driesschaert, E., Fichfet, T., Goosse, H., Renssen, H., 2009. The
effect of dynamic–thermodynamic icebergs on the southern ocean climate in
a three-dimensional model. *Ocean Modelling* 26 (1), 104–113.
- Lefebvre, W., Goosse, H., Timmermann, R., Fichfet, T., 2004. Influence of the
southern annular mode on the sea-ice–ocean system. *Journal of Geophysical
Research: Oceans (1978–2012)* 109 (C9).
- Lenn, Y.-D., Chereskin, T. K., 2009. Observations of ekman currents in the
southern ocean. *Journal of Physical Oceanography* 39 (3), 768–779.
- Lichey, C., Hellmer, H. H., 2001. Modeling giant-iceberg drift under the influence
of sea ice in the weddell sea, antarctica. *Journal of Glaciology* 47 (158), 452–
460.
- Liu, J., Curry, J. A., Martinson, D. G., 2004. Interpretation of recent antarctic
sea-ice variability. *Geophysical Research Letters* 31 (2).
- Madec, G., 2014. NEMO ocean engine, institut pierre-simon laplace (ipsl) Edi-
tion. No. 27 in Note du Ple de modlisation.
- Marsh, R., Ivchenko, V. O., Skliris, N., Alderson, S., Bigg, G. R., Madec,
G., Blaker, A. T., Aksenov, Y., Sinha, B., Coward, A. C., Le Sommer, J.,
Merino, N., Zalesny, V. B., May 2015. NEMO-ICB (v1.0): interactive icebergs
in the NEMO ocean model globally configured at eddy-permitting resolution.

- 730 Geosci. Model Dev. 8 (5), 1547–1562.
 URL <http://www.geosci-model-dev.net/8/1547/2015/>
- Marsland, S., Wolff, J.-O., 2001. On the sensitivity of southern ocean sea-ice to the surface freshwater flux: a model study. *Journal of Geophysical Research: Oceans* (1978–2012) 106 (C2), 2723–2741.
- 735 Martin, T., Adcroft, A., 2010. Parameterizing the fresh-water flux from land ice to ocean with interactive icebergs in a coupled climate model. *Ocean Modelling* 34 (3), 111–124.
- Parkinson, C. L., Cavalieri, D. J., Aug. 2012. Antarctic sea-ice variability and trends, 1979–2010. *The Cryosphere* 6 (4), 871–880.
 740 URL <http://www.the-cryosphere.net/6/871/2012/>
- Penduff, T., Juza, M., Barnier, B., Zika, J., Dewar, W. K., Treguier, A.-M., Molines, J.-M., Audiffren, N., 2011. Sea level expression of intrinsic and forced ocean variabilities at interannual time scales. *Journal of Climate* 24 (21), 5652–5670.
- 745 Peng, G., Meier, W., Scott, D., Savoie, M., 2013. A long-term and reproducible passive microwave sea ice concentration data record for climate studies and monitoring. *Earth System Science Data* 5 (2), 311–318.
- Polvani, L. M., Smith, K. L., Jun. 2013. Can natural variability explain observed Antarctic sea-ice trends? New modeling evidence from CMIP5. *Geophysical Research Letters* 40 (12), 3195–3199.
 750 URL <http://onlinelibrary.wiley.com/biblioplanets.gate.inist.fr/doi/10.1002/grl.50578/abstract>
- Rignot, E., Bamber, J. L., Van Den Broeke, M. R., Davis, C., Li, Y., Van De Berg, W. J., Van Meijgaard, E., 2008. Recent antarctic ice mass loss from radar interferometry and regional climate modelling. *Nature Geoscience* 1 (2), 106–110.
 755
- Rignot, E., Jacobs, S., Mouginit, J., Scheuchl, B., 2013. Ice-shelf melting around antarctica. *Science* 341 (6143), 266–270.
- Rignot, E., Jacobs, S. S., 2002. Rapid bottom melting widespread near antarctic ice sheet grounding lines. *Science* 296 (5575), 2020–2023.
 760
- Schodlok, M., Hellmer, H., Rohardt, G., Fahrbach, E., 2006. Weddell sea iceberg drift: Five years of observations. *Journal of Geophysical Research: Oceans* (1978–2012) 111 (C6).
- 765 Shepherd, A., Ivins, E. R., Geruo, A., Barletta, V. R., Bentley, M. J., Bettadpur, S., Briggs, K. H., Bromwich, D. H., Forsberg, R., Galin, N., et al., 2012. A reconciled estimate of ice-sheet mass balance. *Science* 338 (6111), 1183–1189.

- Silva, T., Bigg, G., Nicholls, K., 2006. Contribution of giant icebergs to the southern ocean freshwater flux. *Journal of Geophysical Research: Oceans* (1978–2012) 111 (C3).
- 770 Stammerjohn, S. E., Martinson, D. G., Smith, R. C., Yuan, X., Rind, D., Mar. 2008. Trends in Antarctic annual sea-ice retreat and advance and their relation to El Niño/Southern Oscillation and Southern Annular Mode variability. *Journal of Geophysical Research* 113 (C3).
URL <http://www.agu.org/pubs/crossref/2008/2007JC004269.shtml>
- 775 Stewart, A. L., Thompson, A. F., 2015. Eddy-mediated transport of warm circumpolar deep water across the antarctic shelf break. *Geophysical Research Letters* 42 (2), 432–440.
- Swart, N., Fyfe, J., 2013. The influence of recent antarctic ice sheet retreat on simulated sea-ice area trends. *Geophysical Research Letters* 40 (16), 4328–4332.
780
- Tournadre, J., Bouhier, N., Girard-Ardhuin, F., Rmy, F., 2015. Large icebergs characteristics from altimeter waveforms analysis. *Journal of Geophysical Research: Oceans* 120 (3), 1954–1974.
- Tournadre, J., Girard-Ardhuin, F., Legrésy, B., 2012. Antarctic icebergs distributions, 2002–2010. *Journal of Geophysical Research: Oceans* (1978–2012) 117 (C05004).
785
- Tournadre J., N. Bouhier, F. G.-A. a. F. R., 2015. Antarctic icebergs distributions 1992-2014. *J. Geophys. Res.*
- Turner, J., Comiso, J. C., Marshall, G. J., Lachlan-Cope, T. A., Bracegirdle, T., Maksym, T., Meredith, M. P., Wang, Z., Orr, A., Apr. 2009. Non-annular atmospheric circulation change induced by stratospheric ozone depletion and its role in the recent increase of Antarctic sea-ice extent. *Geophysical Research Letters* 36 (8), L08502.
790
URL <http://onlinelibrary.wiley.com/biblioplanets.gate.inist.fr/doi/10.1029/2009GL037524/abstract>
795
- Turner, J., Hosking, J. S., Bracegirdle, T. J., Marshall, G. J., Phillips, T., 2015. Recent changes in antarctic sea ice. *Philosophical Transactions of the Royal Society of London A: Mathematical, Physical and Engineering Sciences* 373 (2045), 20140163.
- 800 Uotila, P., Holland, P. R., Vihma, T., Marsland, S. J., Kimura, N., 2014. Is realistic antarctic sea-ice extent in climate models the result of excessive ice drift? *Ocean Modelling* 79, 33–42.
- van den Berk, J., Drijfhout, S., 2014. A realistic freshwater forcing protocol for ocean-coupled climate models. *Ocean Modelling* 81, 36–48.

⁸⁰⁵ Wesche, C., Dierking, W., 2015. Near-coastal circum-antarctic iceberg size distributions determined from synthetic aperture radar images. *Remote Sensing of Environment* 156, 561–569.

Zhang, J., 2007. Increasing antarctic sea-ice under warming atmospheric and oceanic conditions. *Journal of Climate* 20 (11), 2515–2529.

ACCEPTED MANUSCRIPT

Figure 1:

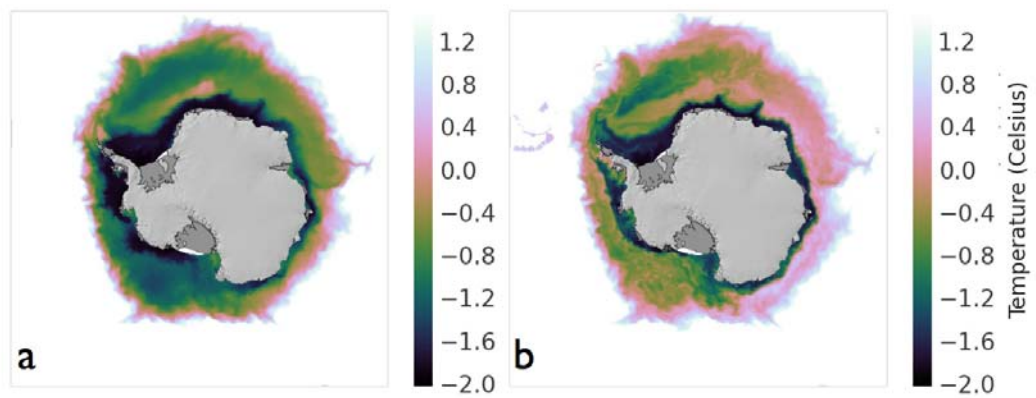


Figure 2:

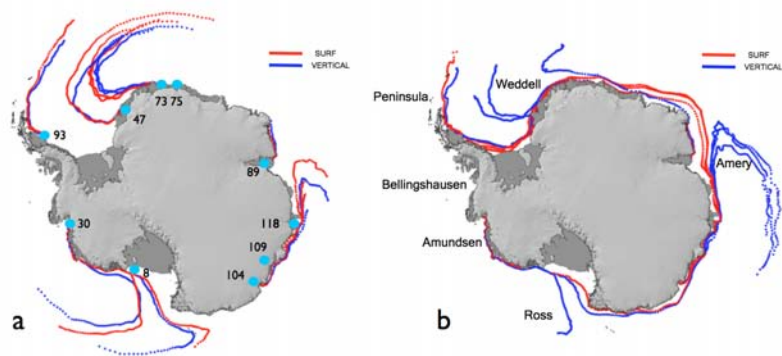


Figure 3:

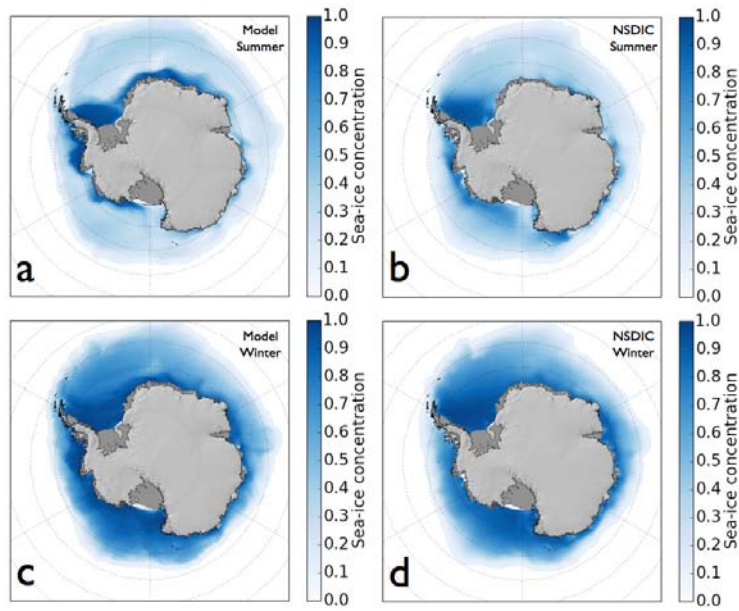
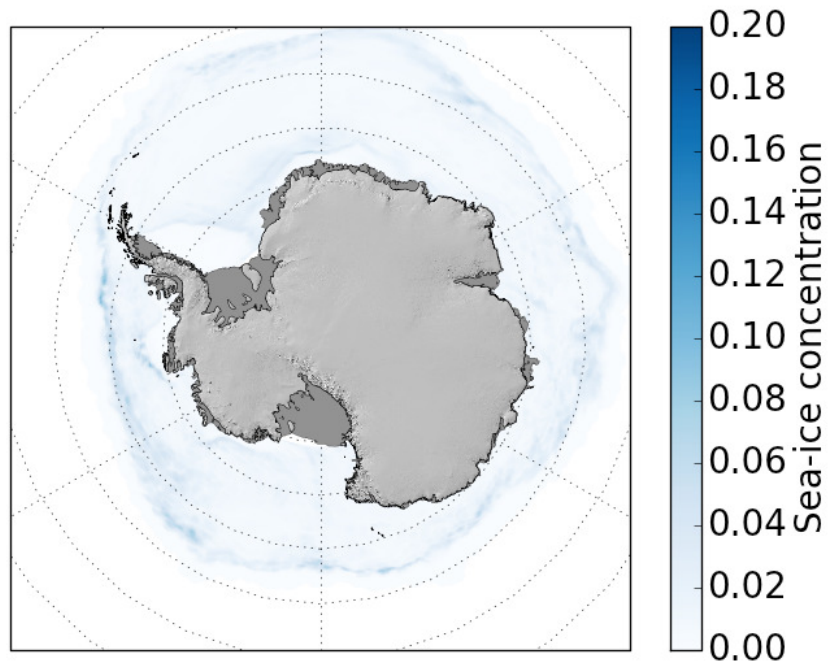


Figure 4:



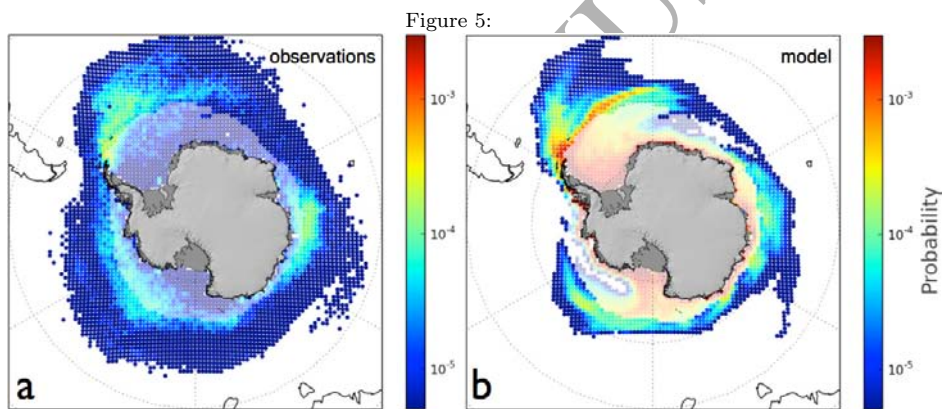


Figure 6:

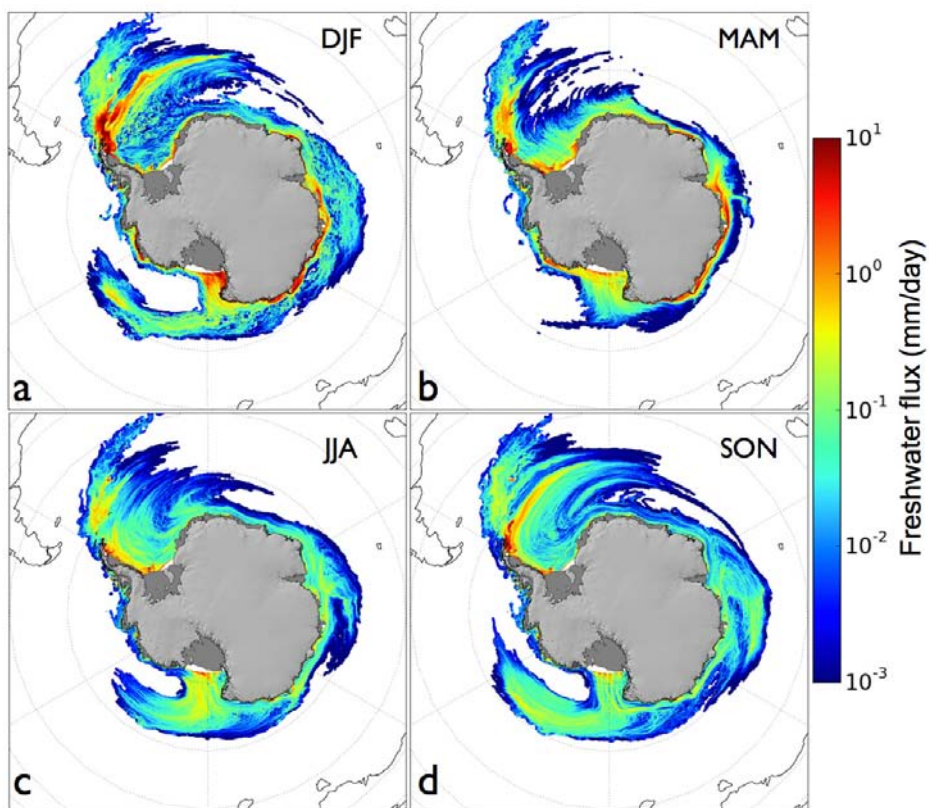


Figure 7:

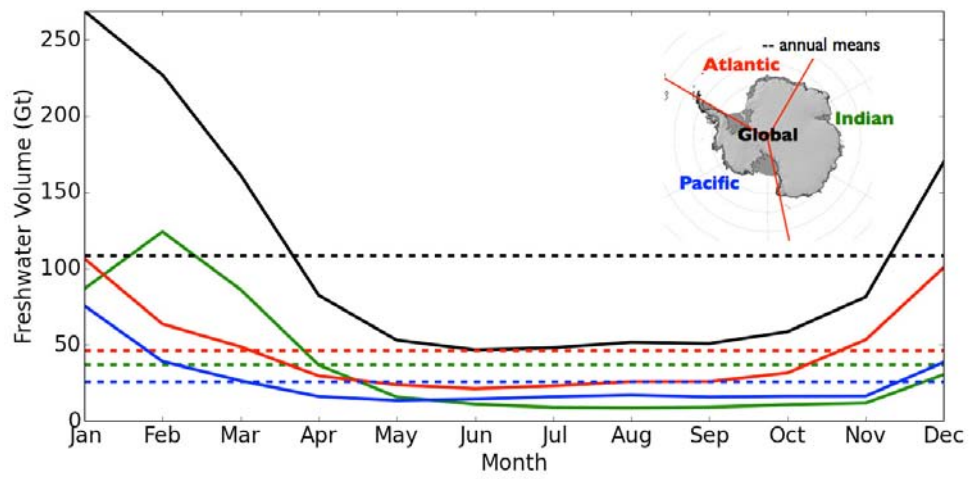


Figure 8:

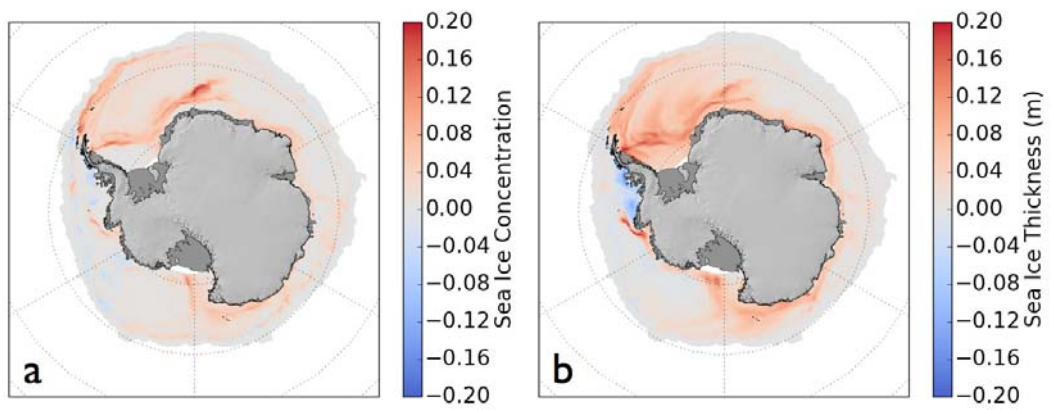


Figure 9:

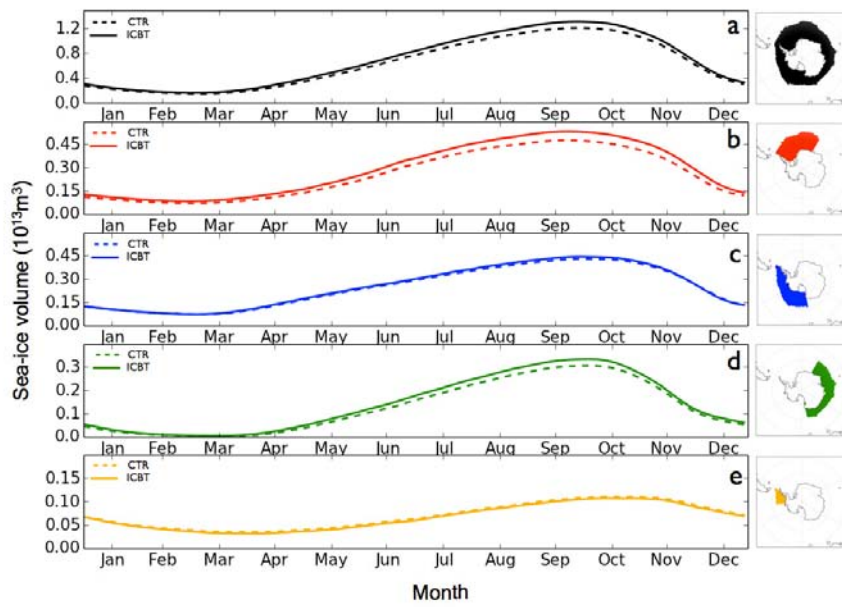


Figure 10:

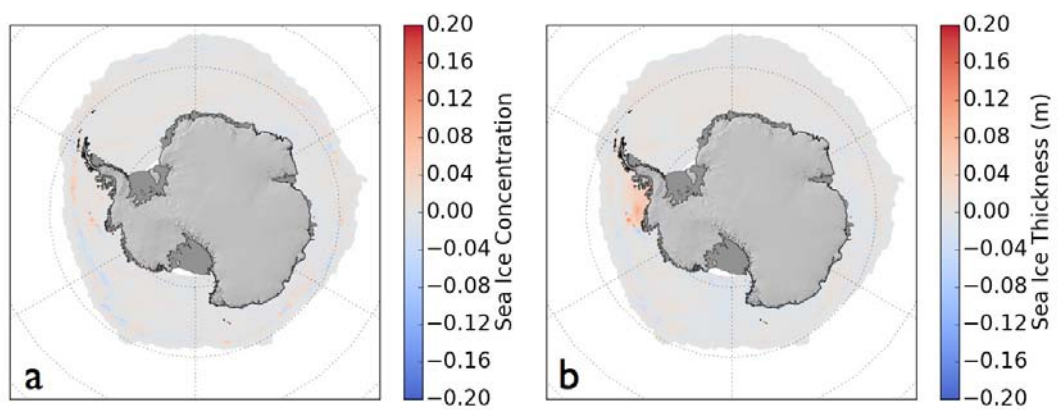


Figure 11:

